

# Cogging Torque Minimization of Surface-Mounted Permanent Magnet Synchronous Machines Using Hybrid Magnet Shapes

Brahim L. Chikouche<sup>1, \*</sup>, Kamel Boughrara<sup>2</sup>, and Rachid Ibtouen<sup>2</sup>

**Abstract**—This paper deals with the magnet pole shape design for the minimization of cogging torque in permanent magnet synchronous machines (PMSM). New shapes of permanent magnet are proposed. The magnet shape is modeled analytically by a set of stacked and well dimensioned layers relatively to the height and opening angle. The final shape of magnet is configured by using three models in view of obtaining lower magnitude of cogging torque. A 2-D exact analytical solution of magnetic field distribution taking into account the shape of magnet, the irregular mechanical thickness of air-gap and semi-closed stator slots is established. The influence of motor's parameters such as the number of stator slots per pole and per phase and PM's magnetization on cogging torque is discussed. Analytical results are validated by the static finite-element method (FEM).

## 1. INTRODUCTION

The cogging torque is one of the very important factors to be predicted in calculating the performance of permanent magnet synchronous machines (PMSMs). It is a pulsating torque due to the interaction of the stator teeth with the rotor magnets.

Several methods have been proposed to reduce the magnitude of cogging torque. Some of them are: the combination of rotor pole pairs and stator slots numbers, the magnetization direction of permanent magnets, magnets and semi-slots opening angles [1], the magnets shape [2–8], stator slots or rotor magnets skewing [9], stator teeth shape [10], fractional number of slots per pole [4], asymmetric distribution of magnets [11] and non-uniform distribution of slots [12]. In particular, the optimum magnet pole shape design has become the most common practice to reduce the cogging torque magnitude.

Electromagnetic torque ripple including cogging torque component causes vibration and acoustic noise in the rotor shaft leading to premature ageing of the electrical machines. In addition, low torque pulsations in motor drives are essential for high-performance speed and position control applications where friendly human-machine interactions are desired.

This paper presents an analytical study of slotted stator permanent-magnets synchronous machines with different shapes of surface mounted magnets. Several studies have been developed to introduce the presence of slots in the analytical calculation directly based on Fourier series analysis and the resolution of Maxwell's equations in slots as in [13–16], or indirectly through using conformal transformation [17] such that the final solution is semi-analytical (hybrid method). L. J. Wu [16] performed a comparative study of four analytical methods applied to the prediction of cogging torque and electromotive force, namely lateral forces method (LF), complex permeance method (PC), the sub-domain method (SD) and the (SD) method based on a single slot per pole. Advantages and disadvantages regarding the quality and the accuracy, besides the computation time of each method, were then cited.

---

*Received 23 November 2014, Accepted 15 January 2015, Scheduled 21 January 2015*

\* Corresponding author: Brahim Ladghem Chikouche (lchbrahim@gmail.com).

<sup>1</sup> Département de Génie Electrique, Faculté de Technologie, Université Mohamed Boudiaf, BP 166 Ichbelia, M'sila, Algeria. <sup>2</sup> Ecole Nationale Polytechnique, ENP, LRE. 10, av. Pasteur, El Harrach, BP182, Algiers 16200, Algeria.

The use of numerical methods for solving problems of electromagnetic fields is a realistic choice. The finite element method is one of the most suitable methods for numerically solving partial differential equations; however, the disadvantage of this method is the associated long computation time especially when attempting to get high accuracy results. It is generally difficult to provide straightforward physical relationships between the performances and parameters. Furthermore, the results obtained by numerical methods are sensitive to the FE meshes, especially for cogging torque, torque ripple, and unbalanced magnetic force.

Compared to other types of motors, PMSMs have been used more and more widely in the fields of industry because of their outstanding advantages of large power density, high efficiency, and excellent characteristics. The structure of a PMSM is determined according to the requirements of its application. A large number of PMSM applications require minimum torque ripple for reduced vibration and acoustic noise, and smooth operation of the motor. Also, low torque pulsations in motor drives are essential for high performance speed and position control applications where friendly human-machine interactions are desired. However, both of a small cogging torque and good motor performance are generally required, while an inappropriate magnet shape can result in an unacceptable high cogging torque, and thus, must be avoided at the design stage. The shape of rotor magnets such as segmentation or beveling has significant influence on the amplitude of cogging torque. The magnet angular width can be optimized to minimize the cogging torque.

The use of sinusoidal permanent magnets (SPM) is one of the solutions to solve the problem of vibration and acoustic noise. The thickness of the ends begins with a zero or some value (see Figure 1), and reaches the thickness of the medium indicated in the specifications. The choice of the thickness of the ends is not usually justified by the authors [2, 5, 11, 21–26] which makes it difficult to optimize.

The characteristics of a permanent-magnet synchronous motor are greatly influenced by the back-electromotive force waveforms in the motor, which are directly related to the magnet shape. The goal is to generate sinusoidal back EMF and constant electromagnetic torque, which would cause, sinusoidal back EMF generation due to the resulting sinusoidal magnetic field distribution.

In this paper, Fourier series expansion and Maxwell's equations are used to determine the analytical expression of cogging torque to analyze the effects of design parameters on cogging torque. Then new structures of rotors are proposed by adopting different magnet shapes. The shape of magnets is configured by combining between the rectangular shape RPM and sinus shape SPM (Figure 1), in view of obtaining lower magnitude of cogging torque. The developed analytical method is used to calculate the cogging torque for three different shapes of magnetic pole. Proof is hereby given that the cogging torque could be greatly reduced.

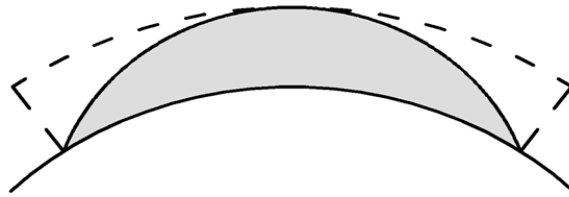


**Figure 1.** Rectangular RPM and sinusoidal SPM permanent magnet shape.

## 2. ANALYZED MOTOR

The analytical calculation of the machines which present complex geometries is a very difficult task because of its inhomogeneous regions leading to a high number of boundary conditions [13]. The stator slotting effect should be considered accurately to predict the magnetic field distribution in the air-gap region of permanent-magnet (PM) motors. A high number of regions can increase the number of equations to be solved and, consequently, the computing times become very long even by using powerful software packages. In all circumstances, the analytical method is the favorite one for the electrical machines design optimization. The mathematical equations contain explicit links between all parameters and considered physical phenomena. This helps the designer to best interpret, through its model, the behavior of the machine, including the interactions between the various parameters.

In order to obtain the solution of magnetic field, the model can be divided into several regions, as shown in Figure 2. In this model, it is assumed that the machine is out of the saturation zone. The study of the electromagnetic field is done in polar coordinates and two-dimensional (2-D), and the magnetic vector potential  $\vec{A}$  has only one component in the axial direction. The rotor and stator iron permeability is assumed to be infinite, and the demagnetization characteristic of the magnet is assumed to be linear. The eddy current losses are assumed to be negligible, the polarization vectors of the permanent magnets perfectly radial, the relative permeability equal to unity, and finally the sides of the slots have a purely radial direction.

The analytical analysis is based on the subdomain method. So, four regions can be considered (Figure 2). The first one contains the magnets and is delimited by the radii  $R_0 \leq r < R_1$  (Figure 3). The second zone is the air-gap between  $R_1 \leq r < R_2$ . The last two regions situated between radii  $R_2 \leq r < R_4$  include all the stator slots. According to Figure 4, the slot can be divided into two regions. The first region (region III) is between  $R_2 < r < R_3$  and represents the slot-opening, where the wedges are placed and which are generally of non-magnetic material type ( $\mu_r = 1$ ). The region IV located between  $R_3 < r < R_4$  is the region where the conductors, also of non-magnetic type, are installed. The study of the field distribution in this machine should be started by modeling the shape of magnets. This can be done by considering the magnet to be composed of a set of piled and well-dimensioned layers, according to the height and opening angle. This is a way to get the desired shape, as shown in Figure 3. The permanent magnet can also be divided vertically into several segments, and the total potential is the sum of all partial potentials due to each segment. This latter study [18] requires a longer computing time than the proposed one especially that regarding dynamic calculation. In the

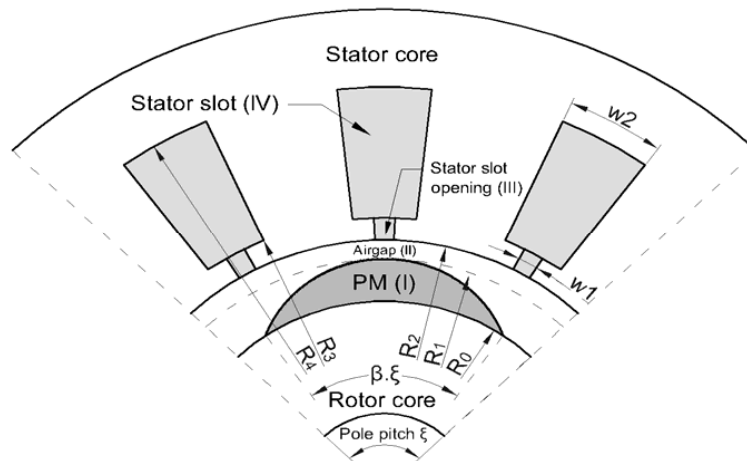


Figure 2. Surface-mounted PM machine with semi-closed slots.

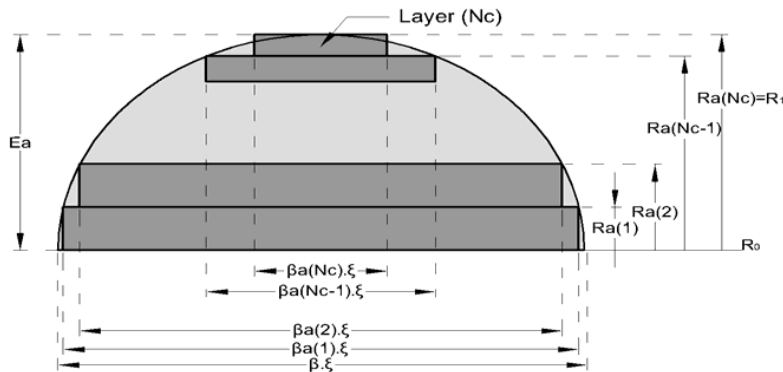
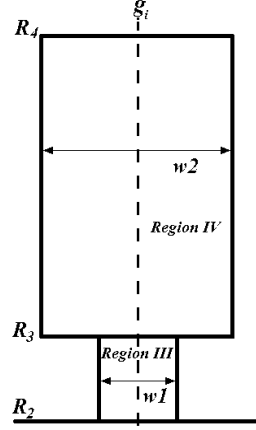


Figure 3. Dividing the magnetic pole into  $N_c$  layers.



**Figure 4.** Representation of the different regions of the  $i$ th stator slot.

first instance, the magnet arc angle ( $\beta \cdot \zeta$ ) of the sinusoidal magnet is divided into  $(N_c + 1)$  pieces with  $\beta a(j)$  opening and where  $N_c$  represents the number of layers. One piece is added to avoid placing the first layer outside the semi-circle, as shown in Figure 3. Radii  $Ra(j)$  are calculated automatically based on the opening angle of the permanent magnet by expression (2), except the final radius  $Ra(N_c)$  which is equal to the outer magnet radius. If the magnet is assumed to consist of infinitely small magnet pieces, the analytical model can be regarded as representing the original single-magnet piece, as shown in light grey color in Figure 3.

$$\beta a(j) = \frac{(N_c + 1 - j) \beta}{N_c + 1} \quad \text{for } j = 1 \dots N_c \quad (1)$$

$$Ra(j) = R_0 + Ea \cdot \cos\left(\frac{\beta a(j) \cdot \pi}{2\beta}\right) \quad (2)$$

where  $\beta$ ,  $\beta a(j)$ ,  $\zeta$  are respectively magnet arc to pole pitch ratio of the entire sinusoidal magnet, magnet arc to pole pitch ratio of the rectangular magnet piece corresponding to layer ( $j$ ), and pole pitch.

### 3. ANALYTICAL SOLUTION OF MAGNETIC FIELD IN THE DIFFERENT SUBDOMAINS

In this paper, an analytical solution of magnetic field distribution based on subdomain method in Surface-Mounted PM motors with semi-closed slots and different magnet shapes is presented. The subdomain method consists in solving directly Maxwell's equations in different subdomains, i.e., air-gap, stator slots and magnets, by the method of variables separation. The magnetic field distribution is obtained in each region by using boundary and interface conditions.

The machine is constituted of four regions. The first one contains the permanent magnets, which results in the resolution of Poisson's equation in polar coordinates. The machine will be studied in no-load operating conditions. For this, the calculation of the field distribution in other regions such as the air-gap or stator slots will be achieved by solving Laplace's equations.

The differential equation in each region is given by

$$\text{Region I: } \nabla^2 A = -\mu_0 (\nabla \times M) \quad (3)$$

$$\text{Regions II, III, IV: } \nabla^2 A = 0 \quad (4)$$

where  $\mu_0$ ,  $M(\theta) = [M_r(\theta), M_\theta(\theta)]$  are respectively the permeability of vacuum and the magnetization of permanent magnet.

Equations (3) and (4) in polar coordinates can be expressed as follows:

For Region I:

$$\frac{\partial^2 A^I(r, \theta)}{\partial r^2} + \frac{1}{r} \frac{\partial A^I(r, \theta)}{\partial r} + \frac{1}{r^2} \frac{\partial^2 A^I(r, \theta)}{\partial \theta^2} = -\frac{\mu_0}{r} \left( M_\theta(\theta) - \frac{\partial M_r(\theta)}{\partial \theta} \right) \quad (5)$$

where  $M_r(\theta)$  and  $M_\theta(\theta)$  are the radial and tangential components of the sinusoidal permanent magnet magnetization.

The tangential magnetization  $M_\theta(\theta)$  is equal to zero in our case where the permanent magnet magnetization is radial.

In the other regions:

$$\frac{\partial^2 A^{II,III,IV}(r, \theta)}{\partial r^2} + \frac{1}{r} \frac{\partial A^{II,III,IV}(r, \theta)}{\partial r} + \frac{1}{r^2} \frac{\partial^2 A^{II,III,IV}(r, \theta)}{\partial \theta^2} = 0 \quad (6)$$

The magnetic flux density and magnetic field vectors  $B$  and  $H$  in these regions are coupled by the following equations:

$$\text{Region I: } B = \mu_0 (H + M) \quad (7)$$

$$\text{Regions II, III, IV: } B = \mu_0 \mu_r H \quad (8)$$

The radial and tangential flux densities are deduced from the magnetic vector potential by:

$$B_r(r, \theta) = \frac{1}{r} \frac{\partial A(r, \theta)}{\partial \theta} \quad (9)$$

$$B_\theta(r, \theta) = -\frac{\partial A(r, \theta)}{\partial r} \quad (10)$$

Solving Laplace equation is usually achieved by exploiting the principle of Euler-Cauchy and Sturm-Liouville, while solving Poisson equation is solved by the method of Green [19]. By taking into account the boundary conditions (11) and (12), the solution of magnetic vector potential in slot region IV can be written as (13).

$$B_{\theta i}^{IV}(r, \theta) = 0|_{r=R_4} \quad (11)$$

$$B_{r i}^{IV}(r, \theta) = 0|_{\theta=g_i \pm w2/2} \quad (12)$$

$$A_i^{IV}(r, \theta) = C_{i2}^{IV} + \sum_{m=1}^{nh} C_{i2m}^{IV} \left( R_4^{-\frac{2m\pi}{w2}} r^{\frac{m\pi}{w2}} + r^{-\frac{m\pi}{w2}} \right) \cdot \cos \left( \frac{m\pi}{w2} (\theta - g_i + w2/2) \right) \quad (13)$$

The solution of magnetic vector potential in slot-opening region III is given, under the boundary condition (14), as follow:

$$B_{r i}^{III}(r, \theta) = 0|_{\theta=g_i \pm w1/2} \quad (14)$$

$$A_i^{III}(r, \theta) = C_{i1}^{III} \ln(r) + C_{i2}^{III} + \sum_{k=1}^{nh} \left( C_{i3k}^{III} r^{\frac{k\pi}{w1}} + C_{i4k}^{III} r^{-\frac{k\pi}{w1}} \right) \cdot \cos \left( \frac{k\pi}{w1} (\theta - g_i + w1/2) \right) \quad (15)$$

The solution of magnetic vector potential in the region II taking into account the periodicity condition at  $2\pi/p$  is given by

$$A^{II}(r, \theta) = \sum_{n=1}^{nh} (C_{3n}^{II} r^{np} + C_{4n}^{II} r^{-np}) \cdot \sin(np \cdot \theta) + \sum_{n=1}^{nh} (C_{5n}^{II} r^{np} + C_{6n}^{II} r^{-np}) \cdot \cos(np \cdot \theta) \quad (16)$$

In the magnet region I, the boundary condition (17)

$$(B_{\theta 1}^I(r, \theta) = \mu_0 M_\theta)|_{r=R_0} \quad (17)$$

and the periodicity condition at  $2\pi/p$  for the magnet having radial magnetization permit to get the magnetic vector potential in the layer ( $j$ ) of permanent magnet as

$$A_j^I(r, \theta) = \sum_{n=1}^{nh} (C_{j3n}^I r^{np} + C_{j4n}^I r^{-np} + \psi_{sj}(r)) \cdot \sin(np \cdot \theta) + \sum_{n=1}^{nh} (C_{j5n}^I r^{np} + C_{j6n}^I r^{-np} + \psi_{cj}(r)) \cdot \cos(np \cdot \theta) \quad (18)$$

where

$$\psi_{sj}(r) = \begin{cases} +\frac{np \cdot M_{rsjn}}{(np)^2 - 1} r & \text{if } np \neq 1 \\ +\frac{M_{rsj1}}{2} r \cdot \ln(r) & \text{if } np = 1 \end{cases} \quad (19)$$

$$\psi_{cj}(r) = \begin{cases} -\frac{np \cdot M_{rcjn}}{(np)^2 - 1} r & \text{if } np \neq 1 \\ -\frac{M_{rcj1}}{2} r \cdot \ln(r) & \text{if } np = 1 \end{cases} \quad (20)$$

$$M_{rsjn} = -\frac{4B_{rm}}{n\pi} \sin\left(\frac{n\pi}{2}\right) \sin\left(\frac{n\pi\beta a(j)}{2}\right) \sin\left(\frac{n\tau}{2}\right) \quad (21)$$

$$M_{rcjn} = -\frac{4B_{rm}}{n\pi} \sin\left(\frac{n\pi}{2}\right) \sin\left(\frac{n\pi\beta a(j)}{2}\right) \cos\left(\frac{n\tau}{2}\right) \quad (22)$$

where  $\psi_{sj}(r)$ ,  $\psi_{cj}(r)$  are the particular solution of (5).  $\tau$  is the relative angular position between the PM and the origin of axis.  $M_{rsjn}$  and  $M_{rcjn}$  are the  $n$ th element of the radial component  $M_{rj}$  of magnet piece layer ( $j$ ).

The radial magnetization  $M_r$  is the sum of the partial radial magnetization  $M_{rj}$  of magnets pieces divided by the number of layers  $N_c$  (see Figure 3).

$$M_{rj} = M_{rsjn} \times \sin(np \cdot \theta) + M_{rcjn} \times \cos(np \cdot \theta) \quad (23)$$

In order to give the final solution of different Equations (13), (15), (16) and (18), the constants  $C^{I,II,III,IV}$  should be determined by applying interface conditions given by:

$$(B_{\theta i}^{IV}(r, \theta) = B_{\theta i}^{III}(r, \theta)) \Big|_{r=R_3}^{g_i - w1/2 \leq \theta \leq g_i + w1/2} \quad (24)$$

$$(B_{r i}^{IV}(r, \theta) = B_{r i}^{III}(r, \theta)) \Big|_{r=R_3}^{g_i - w1/2 \leq \theta \leq g_i + w1/2} \quad (25)$$

$$(B_{r i}^{III}(r, \theta) = B_r^{II}(r, \theta)) \Big|_{r=R_2}^{g_i - w1/2 \leq \theta \leq g_i + w1/2} \quad (26)$$

$$\left( B_{\theta}^{II}(r, \theta) = \sum_{i=1}^{Q_s} B_{\theta i}^{III}(r, \theta) \right) \Big|_{r=R_2} \quad (27)$$

where  $Q_s$  represents the number of stator slots and subscript  $i$  denotes the  $i$ th slot.

$$(B_r^{II}(r, \theta) = B_{rN_c}^I(r, \theta)) \Big|_{r=R_1} \quad (28)$$

$$(B_{\theta}^{II}(r, \theta) = B_{\theta N_c}^I(r, \theta) - \mu_0 M_{\theta}) \Big|_{r=R_1} \quad (29)$$

$$(B_{rj}^I(r, \theta) = B_{r(j+1)}^I(r, \theta)) \Big|_{r=R_{a(j)}} \quad (30)$$

$$(B_{\theta j}^I(r, \theta) = B_{\theta(j+1)}^I(r, \theta)) \Big|_{r=R_{a(j)}} \quad (31)$$

where  $j = [1 \quad N_c - 1]$ .

For a machine having  $2p = 6$ ,  $Q_s = 36$ ,  $\beta = 81\%$  and with dimensions shown in Table 1, the distribution of the radial and tangential flux density in the middle of the air-gap are calculated and plotted in Figure 5. The flux density in the air-gap, the PM layers, the slot-openings and slots regions are computed with a finite number of harmonics as indicated in Table 1. The adopted magnet number of layers is sufficient to consider it shape sinusoidal. The validation by finite element method (FEM) is performed employing the FEMM software package [20]. The number of elements in the air-gap is selected such that the fluctuations on the curves are ignored. Excellent agreement is obtained between analytical and FEM results.

Table 1. Parameters of the studied machine.

Parameter	Symbol	Value and unit
Magnet remanence	$B_{rm}$	1.28 T
Magnet relative permeability	$\mu_r$	1
Magnetization direction	-	Radial
Stator slot-opening span angle	$w_1$	$2^\circ$
Outer rotor radius	$R_0$	57.50 mm
Outer magnet radius	$R_1$	64.00 mm
Stator bore radius	$R_2$	64.65 mm
Outer slot-opening radius	$R_3$	68.65 mm
Outer stator slot radius	$R_4$	92.70 mm
Stack length	$L_u$	150.0 mm
Rotor magnet thickness	$E_a$	06.50 mm
Air-gap length	$e$	00.65 mm
Axial length of the motor	$L_u$	150.0 mm
Layers number of magnet	$N_c$	23
Number of turns per slot	$N_s$	20
Harmonics number	$N_h$	99

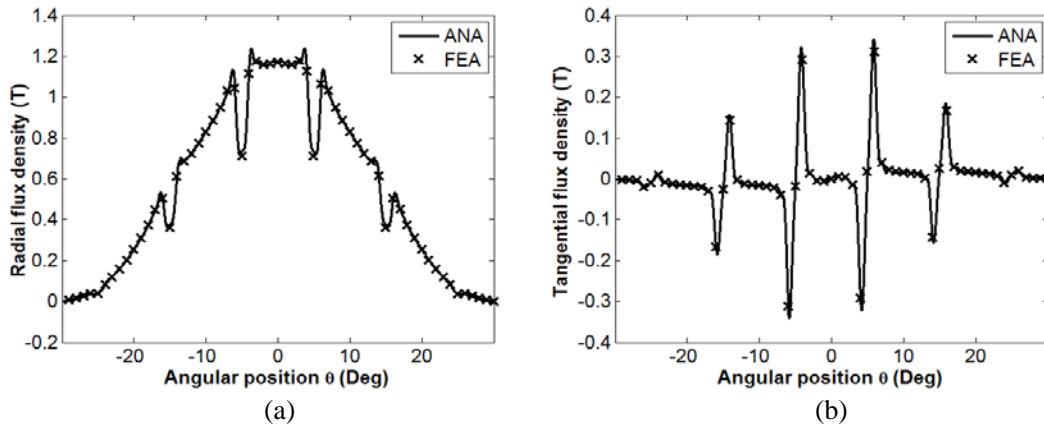


Figure 5. (a) Radial and (b) tangential components of the flux density in the middle of air-gap for  $2p = 6$ ,  $Q_s = 36$ ,  $\beta = 81\%$ .

#### 4. TORQUE AND BACK-EMF CALCULATION

##### 4.1. Cogging Torque

Cogging torque (CT) is due to the modulation of the air-gap flux density and the stator slots. According to Maxwell's stress tensor theory, the cogging torque is calculated using the following relation:

$$T_c = \frac{L_u R^2}{\mu_0} \int_0^{2\pi} B_r^{II}(r, \theta) \times \cdot B_\theta^{II}(r, \theta) \cdot d\theta \tag{32}$$

where  $R$ ,  $L_u$  are respectively the radius of a circle placed at the middle of the air-gap and the axial length of the motor.

## 4.2. Back EMF

The back EMF is the key factor to determine the characteristics of electric machines and that is given by the rate of change of flux linkage according to time variation. The flux linkage can be obtained as follows:

$$\varphi_i^{IV} = \frac{N_s L_u}{S} \int_{g_i-w/2}^{g_i+w/2} \int_{R_3}^{R_4} A_i^{IV}(r, \theta) \cdot r \cdot dr \cdot d\theta \quad (33)$$

where  $S$ ,  $N_s$  are the cross section area of the stator slots and the number of series turns per slot respectively. The flux linkage per phase due to PMs can be expressed as:

$$\psi_{A,B,C}^{IV} = C_m \cdot \varphi_i^{IV} \quad (34)$$

where  $C_m$  is the connecting matrix that represents the distribution of stator windings in the slots.

The three phase's back-EMF can be calculated by:

$$E_{A,B,C} = \Omega_r \frac{d\psi_{A,B,C}^{IV}}{d\tau} \quad (35)$$

where  $\Omega_r$  is the rotor angular speed.

## 4.3. Electromagnetic Torque

The electromagnetic torque ( $T_{em}$ ) can be calculated by integrating Maxwell's stress tensor along a circle with constant radius ( $r$ ) located inside the air-gap or by:

$$T_{em} = \frac{E_A I_A + E_B I_B + E_C I_C}{\Omega_r} \quad (36)$$

The total torque ( $TT$ ) is defined as the sum of electromagnetic torque ( $T_{em}$ ) and cogging torque ( $T_c$ ).

$$TT = T_{em} + T_c \quad (37)$$

## 5. OPTIMAL COGGING TORQUE CALCULATION

In this study, the improvement of the shape of the sinusoidal permanent magnets is sought to minimize the magnitude of the cogging torque. At a first step, the optimal magnet arc to pole pitch ratio  $\beta_{optimal}$  is determined using the first model shown in Figure 2 where the thickness of the ends of the permanent magnet is null. This opening will produce the lowest possible magnitude of cogging torque. If  $\beta$  is satisfied, the process of cutting the ends of the magnet begins, which lasts until a new magnitude corresponding to the new magnet arc to pole pitch ratio  $\alpha$ , as shown in Figure 6, is obtained. This magnitude must be lower or equal to that of the first case.

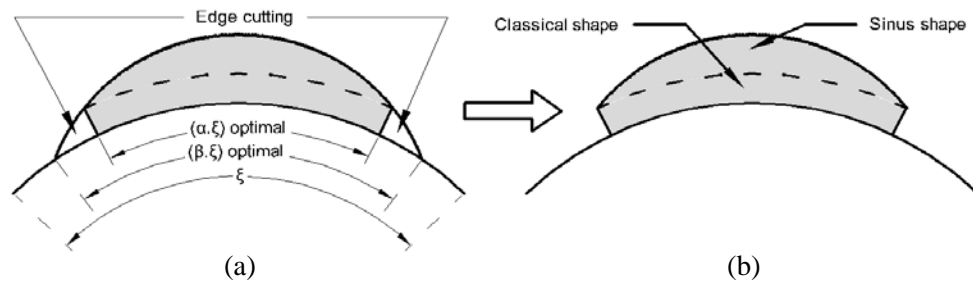


**Figure 6.** First modification of the sinusoidal-shaped magnet, (a) SPM toward, (b) SPM-M1.

### 5.1. Application Examples

For a machine with 6 slots per pole ( $2p = 6$ ) and with the same dimensions of Table 1, the optimal magnitude of cogging torque is found to be 0.2235 Nm when  $\beta = 81\%$ , as shown in Figure 7(a).

Now, considering the second configuration by cutting the extremities of the permanent magnet, the new optimal magnitude occurs for  $\alpha = 65\%$ ; while the magnitude of cogging torque takes the value of 0.1118 Nm, a reduction of about 49.97% in cogging torque is achieved.

The final shape of the magnet consists of two regions, i.e., a simple shape underneath the sinusoidal top part, as shown in Figure 6. Now the lower simple shape can be modified by acting on the magnet arc to pole pitch ratio  $\gamma$ , as in the previous case, so that the final shape is as indicated in Figure 8(a) or

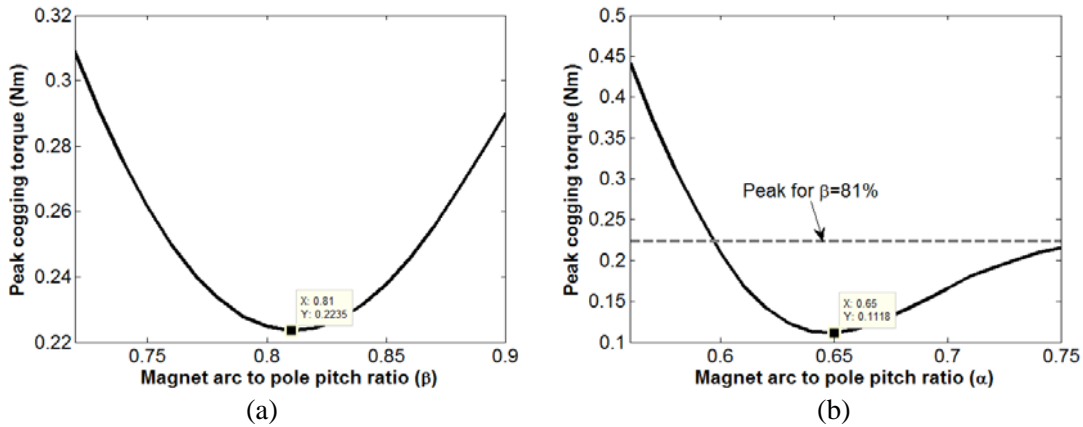


**Figure 7.** Analytically calculated peak cogging torque for different magnet arc to pole pitch ratios, (a)  $\beta$  and (b)  $\alpha$  for  $2p = 6$ ,  $Q_s = 36$ .

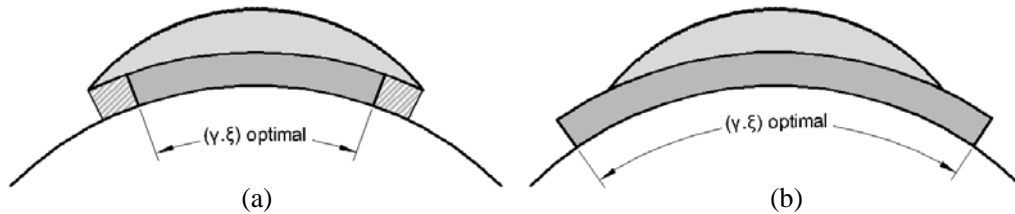


**Figure 8.** Second modification of the sinusoidal-shaped magnet, (a) SPM-M2A, (b) SPM-M2B.

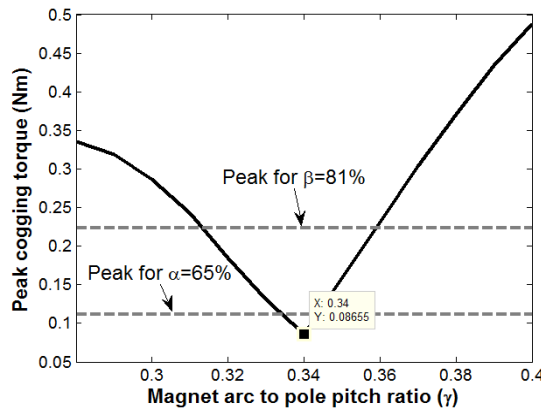


**Figure 9.** Comparative representation of different magnitudes for  $2p = 6$ ,  $Q_s = 36$ ,  $\beta = 81\%$ ,  $\alpha = 65\%$ .

**Table 2.** Analytical results of torque for the 1st, 2nd and 3rd configuration.

	$2p = 6, Q_s = 36$			$2p = 8, Q_s = 72$			$2p = 4, Q_s = 36$			$2p = 4, Q_s = 24$		
	Optimal magnet opening (%)											
	$\beta$	$\alpha$	$\gamma$	$\beta$	$\alpha$	$\gamma$	$\beta$	$\alpha$	$\gamma$	$\beta$	$\alpha$	$\gamma$
	81	65	34	100	65	44	55	42	66	78	69	100
<b>CT optimal (Nm)</b>	<b>0.2235</b>	<b>0.1118</b>	<b>0.0865</b>	<b>0.2989</b>	<b>0.1238</b>	<b>0.0759</b>	<b>0.1332</b>	<b>0.0522</b>	<b>0.0425</b>	<b>0.0687</b>	<b>0.0441</b>	<b>0.0383</b>
$T_{em}$ (mean) (Nm)	1.6329	1.5992	1.3862	4.8503	4.5550	3.8855	0.7990	0.7560	0.8893	0.7120	0.7081	0.7244
$T_{em}$ (ripple) (%)	1.9297	2.8354	2.9904	0.2719	3.5118	0.9934	6.5572	7.9489	2.1829	3.3291	3.7289	2.0840
$TT$ (mean) (Nm)	1.6329	1.5992	1.3863	4.8503	4.5550	3.8855	0.7991	0.7560	0.8893	0.7121	0.7081	0.7244
$TT$ (ripple) (%)	<b>28.992</b>	<b>16.521</b>	<b>15.313</b>	<b>12.421</b>	<b>8.4074</b>	<b>4.7315</b>	<b>38.721</b>	<b>21.648</b>	<b>11.441</b>	<b>23.297</b>	<b>14.890</b>	<b>12.165</b>

**Table 3.** Analytical results for the optimal magnitude of cogging torque.

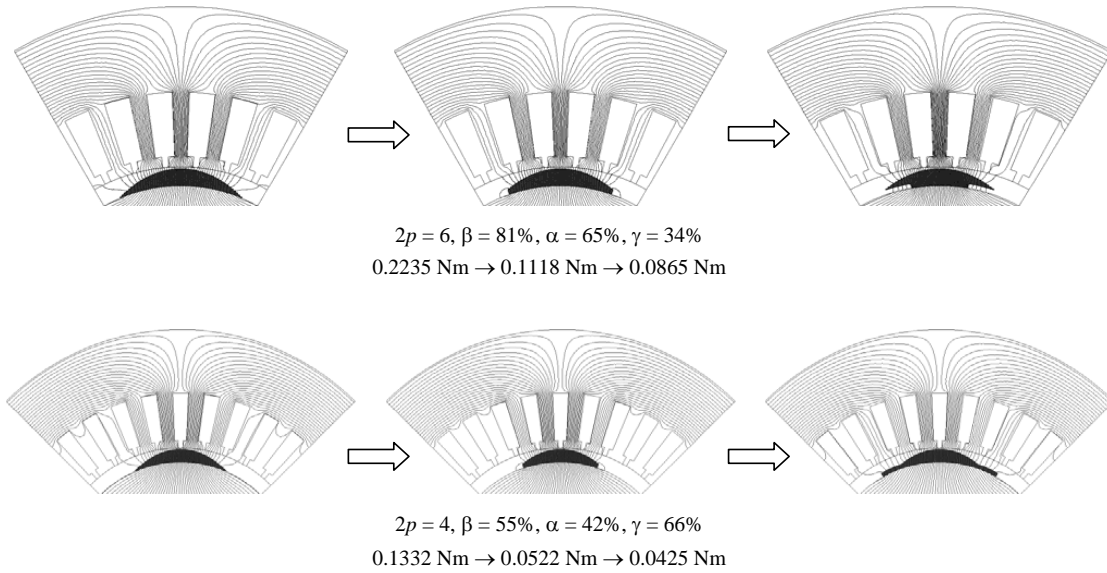
	Machine having SPM-M2 (A or B) (Nm)	Machine having RPM (Nm)	Reduction (%)
$2p = 6, Q_s = 36$	0.0865	1.6654	94.80
$2p = 8, Q_s = 72$	0.0759	2.1113	96.40
$2p = 4, Q_s = 36$	0.0425	1.0850	96.08
$2p = 4, Q_s = 24$	0.0383	0.8597	95.54

Figure 8(b). It is also noticed that the magnet extremities in Figure 8(a) are borne by a nonmagnetic material base, such as aluminum.

If the previous example in which  $2p = 6, Q_s = 36, \beta = 81\%, \alpha = 65\%$  is considered and if the lower opening of magnet is equal to  $\gamma = 34\%$ , it is found that the magnitude of cogging torque decreases from 0.1118 Nm towards 0.0865 Nm. Consequently, another reduction of 22.62% compared to the previous case is reached as shown in Figure 9. Table 2 shows the values of the optimal magnitude of cogging torque (CT) related to the 1st, 2nd and 3rd configuration derived on the basis of the analytical model. These machines have the same dimensions (see Table 1) except the number of slots and poles. The shapes of permanent magnet proposed in this paper are very suitable for minimizing the magnitude of cogging torque (CT) and total torque ripple. Figure 10 shows the optimal shape of permanent magnet in function of the different openings  $\alpha, \beta$  and  $\gamma$ . Generally, the number of steps for calculating the cogging torque does not exceed 10 for any machine dimensions and parameters.

It can be seen that the machine having a SPM-M2 type exhibits good results, as far as cogging torque peak is concerned, compared to the machine having RPM type (see Table 3). This is due to the fact that the radial flux density distribution has a form similar to that of a sinusoid. The difference between those machines is the distribution of the flux density within the air-gap. The field lines, see Figure 11(a), are all distributed over the pole pitch, however, Figure 11(b), shows that the flux lines are concentrated in the teeth forcing the magnetic circuit to be saturated.

In order to make a comparative study between the machine of interest in this paper and machine having RPM type, the current supplying the machine is selected small and equal to 1 A so that the



**Figure 10.** Representation of configuration stages of the magnet shaping and optimal value determination of cogging torque magnitude by analytical method.

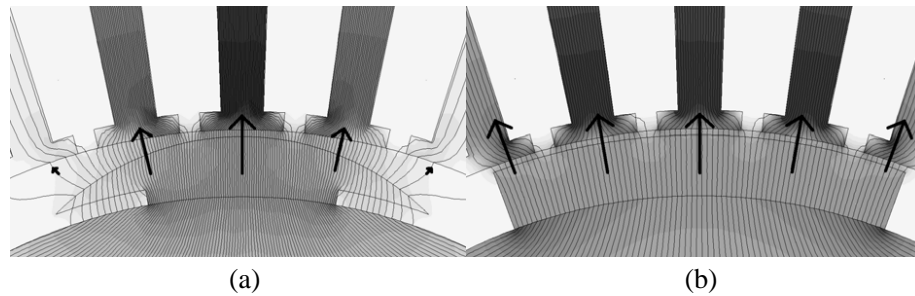


**Figure 11.** Distribution of flux density for a machine having  $2p = 6$ ,  $Q_s = 36$ , (a) SPM-M2A type, (b) RPM type, with optimal magnet opening.

**Table 4.** Analytical results of comparative study between a machine having SPM-M2 (A or B) and RPM.

	$2p = 6, Q_s = 36$		$2p = 8, Q_s = 72$		$2p = 4, Q_s = 36$		$2p = 4, Q_s = 24$	
	SPM-M2A	RPM	SPM-M2A	RPM	SPM-M2B	RPM	SPM-M2B	RPM
<b>CT optimal (Nm)</b>	<b>0.0860</b>	<b>1.6654</b>	<b>0.0759</b>	<b>2.1113</b>	<b>0.0425</b>	<b>1.0850</b>	<b>0.0383</b>	<b>0.8597</b>
$T_{em}$ (mean) (Nm)	1.3862	2.6214	3.8855	6.9263	0.8893	1.7548	0.7244	1.1714
$T_{em}$ (ripple) (%)	2.9904	11.726	0.9934	8.9432	2.1829	9.6885	2.0840	14.201
$TT$ (mean) (Nm)	1.3863	2.6214	3.8855	6.9263	0.8893	1.7548	0.7244	1.1714
<b><math>TT</math> (ripple) (%)</b>	<b>15.313</b>	<b>132.13</b>	<b>4.7315</b>	<b>63.795</b>	<b>11.441</b>	<b>126.97</b>	<b>12.165</b>	<b>149.56</b>

effect of the cogging torque on the total torque ( $TT$ ) will be remarkable. For this purpose, under these conditions, the machine can be compared to the classical machine. Figure 12 shows the back-EMF and electromagnetic torque for a machine having  $2p = 6$  and 36 slots.

Table 4 presents a comparative study between the machine under study and the machine having classical magnets RPM. The classical machine having RPM always presents a total torque ripple very high compared to the machine having SPM-M2 (A or B) whatever the number of slots or poles is and that is justified by the flux density waveform distribution in the air-gap.

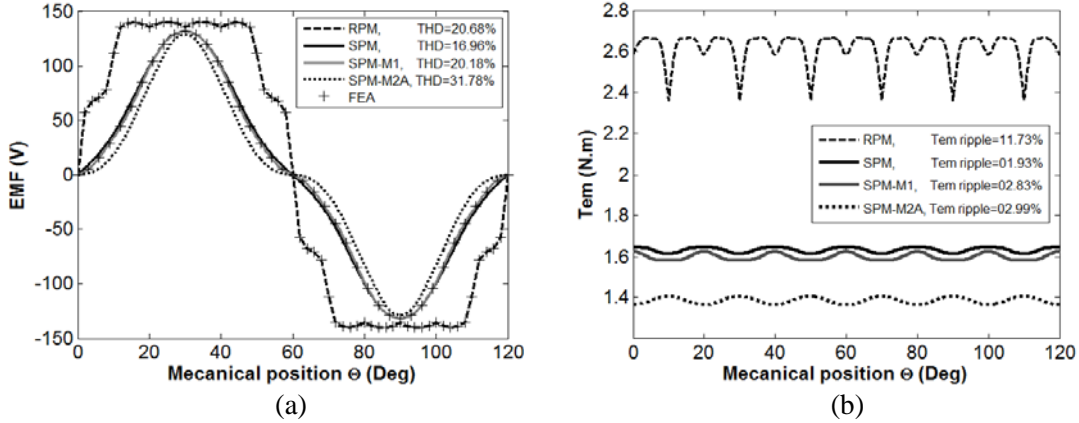


**Figure 12.** (a) Back-EMF and (b) electromagnetic torque for a machine having  $2p = 6$ ,  $Q_s = 36$  after the 1st, 2nd and 3rd configuration stages compared to RPM.

## 6. CONCLUSION

For the majority of industrial applications, reduction of the cogging torque is one of the most important aspects in the PMSMs design. In this paper, cogging torque reduction for PMSM has been analyzed. An analytical method based on the subdomain method has been proposed and the obtained results compared to those derived from the FEM. Attempt has been made to search for various configurations of permanent magnet shape so that the cogging torque magnitude is reduced as much as possible while keeping the same thickness. In fact, the best method is to go through the three presented models while acting on the openings  $\alpha$ ,  $\beta$  and  $\gamma$ . The related cogging torques are then calculated and compared. The proposed magnet shapes, namely SPM-M2A and SPM-M2B, show better characteristics than the conventional RPM or SPM model. Finally, the reduction of the cogging torque is even more pronounced for the structures having a high number of slots per pole.

## REFERENCES

1. Boughrara, K., B. Ladghem Chikouche, R. Ibtouen, D. Zarko, and O. Touhami, "Analytical analysis of slotted air-gap surface mounted permanent-magnet synchronous motor with magnet bars magnetized in shifting direction," *IEEE Trans. Magn.*, Vol. 45, No. 2, 747–758, Feb. 2009.
2. Laskaris, K. I. and A. G. Kladas, "Permanent-magnet shape optimization effects on synchronous motor performance," *IEEE Trans. Ind. Elect.*, Vol. 58, No. 9, 3776–3783, Sep. 2011.
3. Ashabani, M., Y. Abdel-Rady, and I. Mohamed, "Multiobjective shape optimization of segmented pole permanent-magnet synchronous machines with improved torque characteristics," *IEEE Trans. Magn.*, Vol. 47, No. 4, 795–804, Apr. 2011.
4. Pang, Y., Z. Q. Zhu, and Z. J. Feng, "Cogging torque in cost-effective surface-mounted permanent-magnet machines," *IEEE Trans. Magn.*, Vol. 47, No. 9, 2269–2276, Sep. 2011.
5. Islam, R., I. Husain, A. Fardoun, and K. McLaughlin, "Permanent-magnet synchronous motor magnet designs with skewing for torque ripple and cogging torque reduction," *IEEE Trans. Ind. Appl.*, Vol. 45, No. 1, 152–160, Jan./Feb. 2009.
6. Shin, P. S., S. H. Woo, and C. S. Koh, "An optimal design of large scale permanent magnet pole shape using adaptive response surface method with latin hypercube sampling strategy," *IEEE Trans. Magn.*, Vol. 45, No. 3, 1214–1217, Mar. 2009.
7. Chabchoub, M., I. B. Salah, G. Krebs, R. Neji, and C. Marchand, "PMSM cogging torque reduction: Comparison between different shapes of magnet," *First International Conference of Renewable Energies and Vehicular Technology*, 206–211, 2012.

8. Oh, S., S. Min, and J. Hong, "Air gap flux density waveform design of surface-mounted permanent magnet motor considering magnet shape and magnetization direction," *IEEE Trans. Magn.*, Vol. 49, No. 5, 2393–2396, May 2013.
9. Guemes, J. A., A. M. Iraolagoitia, J. I. Del Hoyo, and P. Fernandez, "Torque analysis in permanent-magnet synchronous motors: A comparative study," *IEEE Trans. Energy Convers.*, Vol. 26, No. 1, 55–63, Mar. 2011.
10. Sung, S. J., S. J. Park, and G. H. Jang, "Cogging torque of brushless DC motors due to the interaction between the uneven magnetization of a permanent magnet and teeth curvature," *IEEE Trans. Magn.*, Vol. 47, No. 7, 1923–1928, Jul. 2011.
11. Tudorache, T. and I. Trifu, "Permanent-magnet synchronous machine cogging torque reduction using a hybrid model," *IEEE Trans. Magn.*, Vol. 48, No. 10, 2627–2632, Oct. 2012.
12. Jiang, X., J. Xing, Y. Li, and Y. Lu, "Theoretical and simulation analysis of influences of stator tooth width on cogging torque of BLDC motors," *IEEE Trans. Magn.*, Vol. 45, No. 10, 4601–4604, Oct. 2009.
13. Boughrara, K., T. Lubin, R. Ibtouen, and M. N. Benallal, "Analytical calculation of parallel double excitation and spoke-type permanent magnet motors; simplified versus exact model," *Progress In Electromagnetics Research B*, Vol. 47, 145–178, 2013.
14. Lubin, T., S. Mezani, and A. Rezzoug, "Improved analytical model for surface mounted PM motors considering slotting effects and armature reaction," *Progress In Electromagnetics Research B*, Vol. 25, 293–314, 2010.
15. Dubas, F. and C. Espanet, "Analytical solution of the magnetic field in permanent-magnet motors taking into account slotting effect: No-load vector potential and flux density calculation," *IEEE Trans. Magn.*, Vol. 45, No. 5, 2097–2109, May 2009.
16. Wu, L. J., Z. Q. Zhu, D. A. Staton, M. Popescud, and D. Hawkins, "Comparison of analytical models of cogging torque in surface-mounted PM machines," *IEEE Trans. Ind. Electron.*, Vol. 59, No. 6, 2414–2425, Jun. 2012.
17. Zarko, D., D. Ban, and T. A. Lipo, "Analytical calculation of magnetic field distribution in the slotted air gap of a surface permanent-magnet motor using complex relative air-gap permeance," *IEEE Trans. Magn.*, Vol. 42, No. 7, 1828–1837, Jul. 2006.
18. Tavana, N. R. and A. Shoulaie, "Analysis and design of magnetic pole shape in linear permanent-magnet machine," *IEEE Trans. Magn.*, Vol. 46, No. 4, 1000–1006, Apr. 2010.
19. Jeffrey, A., *Advanced Engineering Mathematics*, University of Newcastle-upon-Tyne, Harcourt/Academic Press, 2002.
20. Meeker, D. C., Finite Element Method Magnetics, Version 4.2, Apr. 2009 Build, <http://www.femm.info>.
21. Li, Y., J. Xing, T. Wang, and Y. Lu, "Programmable design of magnet shape for permanent-magnet synchronous motors with sinusoidal back EMF waveforms," *IEEE Trans. Magn.*, Vol. 44, No. 9, 2163–2167, Sep. 2008.
22. Shah, S. Q. A., T. A. Lipo, and B.-I. Kwon, "Modeling of novel permanent magnet pole shape SPM motor for reducing torque pulsation," *IEEE Trans. Magn.*, Vol. 48, No. 11, 4626–4629, Nov. 2012.
23. Jang, S.-M., H.-I. Park, J.-Y. Choi, K.-J. Ko, and S.-H. Lee, "Magnet pole shape design of permanent magnet machine for minimization of torque ripple based on electromagnetic field theory," *IEEE Trans. Magn.*, Vol. 47, No. 10, 3586–3589, Oct. 2011.
24. Chaithongsuk, S., B. Nahid-Mobarakeh, N. Takorabet, J. P. Caron, and F. Meibody-Tabar, "Optimal design of PM motors to achieve efficient flux weakening strategy in variable speed control applications," *XIX International Conference on Electrical Machines — ICEM*, 1–6, Rome, 2010.
25. Chu, W. Q. and Z. Q. Zhu, "Investigation of torque ripples in permanent magnet synchronous machines with skewing," *IEEE Trans. Energy Convers.*, Vol. 49, No. 3, 1211–1220, Mar. 2013.
26. Shen, Y. and Z. Q. Zhu, "Analysis of electromagnetic performance of Halbach PM brushless machines having mixed grade and unequal height of magnets," *IEEE Trans. Energy Convers.*, Vol. 49, No. 4, 1461–1469, Apr. 2013.